

Cite as: C. S. Rustomji *et al.*, *Science*
10.1126/science.aal4263 (2017).

Liquefied gas electrolytes for electrochemical energy storage devices

Cyrus S. Rustomji,¹ Yangyuchen Yang,² Tae Kyoung Kim,² Jimmy Mac,¹ Young Jin Kim,² Elizabeth Caldwell,² Hyeseung Chung,¹ Y. Shirley Meng^{1*}

¹Department of Nano Engineering, University of California, San Diego, La Jolla, CA 92121, USA. ²Department of Mechanical and Aerospace Engineering, Materials Science and Engineering Program, University of California, San Diego, La Jolla, CA 92121, USA.

*Corresponding author. E-mail: shmeng@ucsd.edu

Electrochemical capacitors and Li-ion batteries have seen little change in their electrolyte chemistry since their commercialization which has limited improvements in device performance. Combining superior physical and chemical properties and a high dielectric-fluidity factor, the use of electrolytes based on solvent systems which exclusively use components which are typically gaseous under standard conditions show a wide potential window of stability and excellent performance over an extended temperature range. Electrochemical capacitors using difluoromethane show outstanding performance from -78 to +65°C with an increased operation voltage. The use of fluoromethane shows a high coulombic efficiency of *ca.* 97% for cycling lithium metal anodes, together with good cyclability of a 4 V lithium cobalt oxide cathode and operation as low as -60°C with excellent capacity retention.

Electrochemical energy storage devices, such as electrochemical capacitors and batteries, are crucial components in everything from communications to transportation. Aqueous based electrolytes have been used for well over a century, but a substantial increase in the energy density was achieved through the development and use of electrolytes based on organic solvents which allowed for operation at higher voltages. The modern Li-ion battery was only realized with a serendipitous discovery that the use ethylene carbonate, a solid at room temperature, as an electrolyte solvent could stabilize the graphite anode via formation of a suitable solid electrolyte interphase (SEI) and allow for reversible lithiation and delithiation of the electrode (*I*). While the majority of electrolyte work remains with liquid solvents and solid electrolyte systems, there has been very little work using electrolyte solvents that are typically gaseous under standard conditions. While not used as an electrolyte, sulfur dioxide ($T_b = -10^\circ\text{C}$) (2) and sulfuryl chloride fluoride ($T_b = +7.1^\circ\text{C}$) (3) have been used as catholytes in non-rechargeable primary lithium batteries, however, both use additional cosolvents in the electrolyte which are liquid at room temperature. There have also been a number of studies using ammonia ($T_b = -33.3^\circ\text{C}$) as a liquid anode due to its ability to solvate alkali metals (4–6).

It is often assumed that materials which are gaseous at room temperature are typically non-polar and have low intermolecular attraction, which prevents them from condensing at room temperature or even solubilizing salts in a cooled, or pressurized, liquid state. While this may be true in general, there are a number of reasonably polar molecules which show low London dispersion forces due to their

small molecular size and are gaseous at room temperature. For instance, the dielectric constant of dichloromethane ($\epsilon_{\text{DCM},20^\circ\text{C}} = 8.9$, $T_b = +40^\circ\text{C}$) is substantially lower than that of structurally similar difluoromethane ($\epsilon_{\text{DFM},20^\circ\text{C}} = 14.2$, $T_b = -52^\circ\text{C}$), although at room temperature the former is a liquid while the latter is a gas. At low temperatures or with moderate pressures, these types of polar gasses may be liquefied and have been shown to be capable of solubilizing salts to form liquefied gas electrolytes, in which ion transport, redox phenomena and other fundamental studies have been conducted (7–13).

The use of liquefied gas electrolyte systems exclusively composed of solvents which are gaseous at room temperature and atmospheric pressure in rechargeable energy storage systems is explored. Although a number of potential liquefied gas solvents were evaluated, efforts were focused on hydrofluorocarbons, which have moderate dielectric constants that allows for the solubility of salts to form conductive electrolytes. These electrolytes show ultra low-temperature operation, increased energy density in electrochemical capacitors and high lithium plating and stripping efficiency for potential use of the high capacity lithium metal anode in batteries. It should be cautioned that while the hydrofluorocarbon solvents themselves are generally non-toxic, they do range from non-flammable to highly flammable and combustion products may be toxic to humans. Further, these solvents do exhibit a low to high global warming potential. As such, these materials should be handled properly with additional information provided in supplementary text.

Physical and chemical properties of liquefied gas solvents

The electrochemical stability for a range of liquid and liquefied gas solvents was qualitatively estimated by calculating the ionization potential and electron affinity of the solvents, shown in Figure S1 and Table S1. Selecting from the solvents with optimal electrochemical stability and polarity, six promising liquefied gas solvents were identified and are compared with conventional liquid solvents in Fig. 1A. In general, these liquefied gas solvents show improved oxidation and reduction resistance compared to conventional solvents. In particular, these calculations suggest fluoromethane (FM) and difluoromethane (DFM) would have improved electrochemical stability over tetrahydrofuran (THF) and ethylene carbonate (EC) which are known for their high stability at highly reductive and oxidative potentials, respectively. Electrostatic potential maps are overlaid on the physical structures of these solvents for comparison in Fig. 1B, which may be used as a tool to qualitatively determine electrochemical reduction stability of solvents. The regions of highest electrostatic potential (bluest regions) increases in the order of THF < FM < DFM < EC, which correlates well to the high electrochemical reduction stability of THF and indicates FM should similarly have good reduction stability. The regions of lowest electrostatic potential (reddest regions) increases in the order of EC < THF < FM < DFM, which correlates well with the high solubility for the relatively small Li⁺ cation in EC and THF and indicates the solubility would be better in FM than DFM.

The dielectric constant of the gaseous solvents (*ca.* $\epsilon = 10 \sim 15$) is significantly lower than conventional liquid solvents which may limit their ability to solubilize various salts. However, the room temperature viscosities of the liquefied gas solvents are also significantly lower than conventional liquid solvents. These properties for the liquefied gas solvents fluoromethane and difluoromethane are compared in Fig. 1C. Both fluoromethane and difluoromethane have a liquid viscosity about three times lower than acetonitrile, which is commonly used in high power devices such as electrochemical capacitors. Because of their exceptionally low viscosities, it is expected that the ion mobility is quite high in electrolytes composed of these solvents. As a qualitative measure of the electrolytic conductivity for a range of solvents, the ratio of dielectric constant to viscosity ($\epsilon_r \cdot \eta^{-1}$), or the solvent dielectric-fluidity factor, is compared in Fig. 1C. It is found that the liquefied gas solvents have a superior dielectric-fluidity factor compared to conventional liquid solvents, including acetonitrile, which generally shows some of the highest electrolytic conductivities (14). This qualitative comparison demonstrates that relatively high electrolytic conductivities may be expected in these solvents having only moderate dielectric constants. Further, the viscosities

of these solvents remain favorable at very low temperatures, as shown in Figure S2, which may allow for high electrolytic conductivity at temperatures where conventional solvents may freeze.

Vapor pressure curves of the six liquefied gas solvents studied over a range of temperatures are moderate and compared in Fig. 1D. Of the solvents studied, fluoromethane and difluoromethane have the highest vapor pressures of 3.8 and 1.8 MPa, respectively, at +25°C. The melting points for each of the solvents are below -100°C. While the boiling points of these solvents are all below room temperature, the present study utilizes these solvents while they are liquefied under their own vapor pressure in a hermetically sealed cell, allowing for electrolyte and cell characterization at increased temperatures where the solvent would normally be gaseous. Further, these solvents have fairly accessible supercritical points, as detailed in Table 1. Having zero surface tension in the super-critical phase, these solvents may provide additional advantages such as superior wetting or access to nano pores in high surface area electrodes (15).

Electrolytic conductivity measurements

Electrolytic conductivity measurements of the liquefied gas electrolytes were conducted in order to determine the most promising solvents. Various liquefied gas solvents and salts were tested over a range of temperatures and it was found that these electrolytes do not follow typical conductivity vs. temperature curves. Generally, the electrolytic conductivity for a liquid electrolyte will scale approximately linearly with increasing temperature, due to decreasing solvent viscosity. However, the liquefied gas electrolytes show three distinct regions of conductivity over a wide range of temperatures, as shown in Fig. 2A for 0.1 M TBAPF₆ (tetrabutylammonium hexafluorophosphate) in difluoromethane. The first region at lower temperatures shows the typical increasing conductivity with increasing temperature, which is due to the decreasing viscosity with increasing temperatures ($\eta_{\text{DFM},-60^\circ\text{C}} = 0.31 \text{ mPa}\cdot\text{s}$, $\eta_{\text{DFM},+20^\circ\text{C}} = 0.12 \text{ mPa}\cdot\text{s}$ (16)). At moderate temperatures, there is a clear maximum followed by a gradual decrease in conductivity. As the solvent approaches the super-critical point ($T_{\text{c,DFM}} = +78^\circ\text{C}$), a drop in conductivity is expected (17) and occurs due to the decreasing dielectric constant lowering the ion mobility ($\epsilon_{\text{DFM},-57^\circ\text{C}} = 28.2$, $\epsilon_{\text{DFM},+20^\circ\text{C}} = 14.2$ (18, 19)). While all solvents generally show a decreasing dielectric constant with increasing temperature, the studied solvents already have a comparably low dielectric constant at room temperature and would be susceptible to considerable ion pairing at increasing temperatures. At even higher temperatures, an abrupt change in the conductivity is observed, which separates the second and third regions of the conductivity curve. Because this sharp change occurs at temperatures considerably lower than the super-critical point, any related

phenomena are not thought to contribute to this behavior. It was found that this abrupt change in electrolytic conductivity is concurrent with a sudden increase in the pressure of the electrolyte solution, beyond the normal solvent vapor pressure. This phenomenon may be explained by considering the thermal expansion behavior of the solvent. In practice, nearly the entire volume of measurement cell is filled at a low temperature with liquid solvent, while a small volume remains open, which is naturally filled with gaseous solvent through thermal evaporation. As the temperature increases, the volume of liquid phase increases due to thermal expansion ($\rho_{\text{DFM},-60^\circ\text{C}} = 1.24 \text{ g}\cdot\text{cc}^{-1}$, $\rho_{\text{DFM},+20^\circ\text{C}} = 0.98 \text{ g}\cdot\text{cc}^{-1}$ (16)) and the volume of the vapor phase decreases. At an elevated temperature, the thermal expansion of the solvent will cause the liquid phase to occupy the entire volume of the cell and any further increase in temperature will result in an isochoric increase in pressure due to the compression of the liquefied gas electrolyte. It should be cautioned that rather high pressures may be observed if solvent thermal expansion is restricted considerably. An increase in pressure on difluoromethane can increase the dielectric constant of the solvent quite dramatically (20). Therefore, it may be understood that the abrupt change in electrolytic conductivity in the third region relative to second region of Fig. 2A is due to an improvement in ion mobility from the increased dielectric constant of the solvent, which results from the increased pressure on the electrolyte system. While this pressure induced effect may be generalized to all electrolytes, it is a particularly significant effect due to the already moderate dielectric constant and high compressibility of this solvent.

Similar electrolytic conductivity phenomena may be observed for the other liquefied gas electrolyte systems explored. The electrolytic conductivity of 0.1 M EMITFSI (1-Ethyl-3-methylimidazolium bis(trifluoromethylsulfonyl)imide) in multiple liquefied gas solvents is shown in Fig. 2B and decreased in the order of difluoromethane, fluoromethane, 1,1-difluoroethane, fluoroethane, 2-fluoropropane, and 1,1,1,2-tetrafluoroethane. This follows the order of decreasing dielectric-fluidity factors for the solvents described previously in Table 1, which gives credibility to the simple qualitative model proposed (the dielectric constants for fluoroethane and 2-fluoropropane were unavailable in the literature). Since difluoromethane was found to exhibit the highest electrolytic conductivity, various salts were tested in this solvent, shown in Figure S3. It was found that TBAPF₆ exhibited the highest electrolytic conductivity in difluoromethane and further studies of this electrolyte system were studied with various concentrations of salt, shown in Fig. 2C. There is a considerable increase in the conductivity of the liquefied gas electrolyte from a concentration of 0.02 to 0.50 M TBAPF₆, which shows the salt

has good solubility in difluoromethane despite its relatively low dielectric constant. The electrolytic conductivity of the 0.50 M solution shows a maximum conductivity of 31 mS·cm⁻¹ at +30°C. More notable, however, is the excellent low-temperature conductivity of 13 mS·cm⁻¹ at -60°C. Previous work showed the optimization of binary mixtures of liquid based solvents with close attention to the conductivity, melting points and potential window, and demonstrated a similar electrolytic conductivity at -60°C for 0.75 M TEABF₄ (tetraethylammonium tetrafluoroborate) in acetonitrile: methyl formate 3:1, however, the potential window of this electrolyte was limited (21). Figure 2C shows that at various concentrations, the conductivity curves exhibit the same general three-regions of electrolytic conductivity across the temperatures measured. A distinct change in the slope of the conductivity curve in the first region, most notably at a concentration of 0.5 M TBAPF₆, is thought to be due to increasing ion pairing which is expected to occur in these moderate dielectric solvents with high salt concentrations. There is a gradual change in the temperature separating the second and third regions, which increases from +35°C to +79°C from a salt concentration of 0.02 M to 0.5 M. This may be understood by the lower thermal expansion coefficient of the solution with increasing salt concentration, which would require more thermal energy to volumetrically expand and create the isochoric increase in pressure, in turn resulting in the abrupt change in conductivity.

While difluoromethane was shown to have an exceptionally high electrolytic conductivity with many salts, it was found that this solvent was unable to solubilize lithium salts. This is likely due to the steric hindrance of the highly electronegative fluorine atoms of adjacent solvent molecules preventing formation of a solvation shell around the Li⁺ cation. Further work showed that lithium bis(trifluoromethane)sulfonimide (LiTFSI) could only be solubilized in the mono-fluorinated liquefied gas solvents; fluoromethane, fluoroethane, and 2-fluoropropane. This is in agreement with previous work which also suggested these mono-fluorinated solvents have an increased basicity and binding energy to the Li⁺ cation over difluoromethane (22) and with the previously discussed electrostatic potential maps of the solvents in Fig. 1B. The electrolytic conductivities of these three mono-fluorinated liquefied gas solvents with 0.1 M LiTFSI are compared in Fig. 2D. Fluoromethane is shown to have the highest electrolytic conductivity of the three solvents, as is expected from the exceptionally high dielectric-fluidity factor. A maximum conductivity of 1.2 mS·cm⁻¹ is seen at -22°C and an impressive low temperature conductivity of 1.1 mS·cm⁻¹ at -60°C. For comparison, a low temperature electrolyte using LiPF₆ in a mixture of carbonates and methyl acetate had an electrolytic conductivity of 0.6 mS·cm⁻¹ at -60°C, but it had rela-

tively poor performance in a full cell due to the non-ideal solvent system (23). The electrolytic conductivity at higher concentrations saw little improvement with the LiTFSI salt. At higher temperatures, there is a sudden drop in conductivity due to the precipitation of the salt out of the electrolyte as fluoromethane reaches its critical temperature ($T_{c,FM} = +44^{\circ}\text{C}$), which is a useful safety feature among lithium based electrolytes.

Electrochemical capacitors

Since difluoromethane shows the highest electrolytic conductivity for non-lithium based salts, the electrochemical stability of this solvent was studied. Figure 3A shows the cyclic voltammetry curves for 0.1 M TEABF₄ in difluoromethane at both +25°C and -60°C. At +25°C, a potential window of 5.70 V is observed. The positive potential limit of 2.47 V vs. Pt matches well with that of anion oxidation (7). A significant reduction current is observed with an onset potential of -3.23 V vs. Pt which results in the continuation of a high reduction current in the reverse sweep direction, possibly due to corrosion of the working electrode. These potential limits are in good agreement with previous results with a similar salt system (7). At -60°C, the electrolyte shows an impressive electrochemical window of 6.83 V, which is wider than that at +25°C due to slower chemical kinetics at the decreased temperatures.

Commercial electrochemical capacitors of 350 F rated capacitance were tested with 0.5 M TEABF₄ in difluoromethane and with a standard liquid electrolyte composed of 1 M TEABF₄ in acetonitrile for comparison, both of which were tested under identical mechanical cell conditions and submerged in electrolyte. The capacitance and resistance over a range of temperatures is shown in Fig. 3B. At +25°C, the capacitance for both devices is *ca.* 375 F and remains fairly constant over the temperature range studied, with only a small decrease to *ca.* 350 F at low temperatures. The resistance of 8.5 and 11.0 mΩ for the difluoromethane and acetonitrile devices, respectively, at +25°C emphasizes the high electrolytic conductivity and applicability of the electrolyte to electrochemical capacitors for high power applications. At low temperatures, while the acetonitrile based device steadily increased in resistance to 14.9 mΩ at -40°C, just above its freezing point, the difluoromethane based device decreases in resistance to 5.8 mΩ at -20°C. This is in agreement with the electrolytic conductivity measurements which show a maximum in electrolytic conductivity around this temperature range. At lower temperatures, the resistance slowly increases, yet is still comparable at -78°C and +25°C, highlighting the excellent low-temperature performance of the electrolyte. This operation temperature is nearly 40°C lower than commercial acetonitrile based electrochemical capacitors are rated for and is unsurpassed by other low-temperature electrolyte formulations (24). At an

elevated temperature of +65°C, the resistance increases only slightly to 13.4 mΩ. Device cycling performance was also studied with difluoromethane in the super-critical phase, shown in Figure S4. Though the capacitance of the device is maintained, there is a substantial increase in electrolyte resistance at +90°C (*ca.* 1500% increase) as the salt precipitates out of the solvent due to the decreasing dielectric constant. When the temperature is lowered, the resistance decreases to nominal as the salt is solubilized back into solution and shows a slight decrease in capacitance due to accelerated cell degradation at the high temperature.

To determine if the novel difluoromethane based electrolyte offers any advantage in terms of energy density, electrochemical capacitors were tested at an elevated voltage and temperature of 3.0 V and +65°C for over 1500 hours, shown in Fig. 3C. The device using the acetonitrile based electrolyte rapidly fails under these accelerated conditions, showing a substantial increase in resistance and decrease in capacitance, which agrees with previous studies of electrochemical capacitors under similar conditions (25). The difluoromethane device, however, shows little decrease in capacitance or increase in resistance under identical conditions. Similarly, a 3.0 V test was carried out at -60°C to test the low temperature life of the device and shows nearly no change in capacitance or resistance. With a comparable capacitance already demonstrated, the increased voltage rating from 2.7 V (for typical acetonitrile devices) to 3.0 V is equivalent to a 23% increase in energy density which offers an advantage for a range of electrochemical capacitor applications such as cold engine cranking, start-stop vehicles and hybrid buses.

Rechargeable lithium metal battery

Due to the high reduction potential of lithium (-3.04 V vs. NHE) a thin electrically insulating, but Li-ion conducting solid electrolyte interphase on the lithium metal instantaneously forms when in contact with many commonly used liquid solvents. Optical images of the resulting chemical products after soaking lithium metal in each of the liquefied gas solvents are shown in Figure S5. The poly-fluorinated solvents (difluoromethane, difluoroethane and 1,1,1,2-tetrafluoroethane) each form a stable SEI on lithium metal preventing further decomposition of the lithium metal or solvent. Though thorough characterization of these interfaces was not done on these chemical products, the SEI is thought to be significantly made up of various fluoropolymers. The mono-fluorinated solvents (fluoromethane, fluoroethane, 2-fluoropropane), which are capable of solubilizing lithium salts, each fully decompose lithium metal into a powder form and no stable SEI is formed. As detailed in Table S2, the reaction time for the full decomposition of lithium metal at room temperature in liquid fluoromethane is significantly slower than in liquid

fluoroethane or 2-fluoropropane. The chemical reduction of fluoromethane by lithium metal is hypothesized to follow as

- 1) $\text{CH}_3\text{F} + \text{Li} \rightarrow \text{LiF} + \text{CH}_3^\cdot$
- 2) $\text{Li} + \text{CH}_3^\cdot \rightarrow \text{CH}_3\text{Li}$
- 3) $\text{CH}_3^\cdot + \text{CH}_3^\cdot \rightarrow \text{C}_2\text{H}_6$

Evidence for LiF and CH_3Li among the chemical products is seen in the x-ray diffraction (XRD) and fourier transform infrared spectroscopy (FTIR) spectra shown in Figure S6 and Figure S7, respectively, which supports this reaction scheme. Since the kinetics for lithium decomposition in fluoromethane are relatively slow, and it is this solvent which had the highest electrolytic conductivity with lithium salts as seen in Fig. 2D, methods to stabilize the surface of lithium metal were explored. It was found the use of carbon dioxide in additive amounts in fluoromethane was sufficient enough to stabilize the lithium surface, due to the creation of a stable lithium carbonate surface layer. The formation of this stable interface is shown in Figure S6 and Figure S7, which show little evidence for LiF or CH_3Li in the SEI layer on the macroscopic level with the addition of 5 wt% carbon dioxide. Carbon dioxide is an effective additive for use in Li-ion batteries (26) but solubility in common organic solvents is limited to *ca.* 0.5 wt% and strongly dependent with temperature (27). Conversely, carbon dioxide and fluoromethane are miscible solvents (28) and may enable the use of this highly effective additive in next generation batteries.

With the addition of carbon dioxide to form a stable SEI layer on lithium metal, the electrochemical stability of the fluoromethane based liquefied gas electrolyte was determined by cyclic voltammetry, shown in Fig. 4A and in more detail in Figure S8. The electrolyte is limited by oxidation at 5.57 and 5.79 V vs. Li at +25°C and -60°C, respectively, which is indicative of slower solvent oxidation kinetics at decreased temperatures. Carbon dioxide reduction is seen to begin at 2.1 V vs. Li, which matches well with the literature (29). Typical lithium metal plating and stripping peaks are observed to be centered around 0 V vs. Li. While the cathodic upper potential deposition peaks for lithium and platinum alloying are not observed due to concurrent carbon dioxide reduction, two anodic upper deposition potential stripping peaks are observed; a larger peak followed by a smaller peak at 0.58 and 1.32 V vs. Li, respectively. At -60°C, a relatively high over potential for lithium nucleation is also observed, with lithium deposition starting at -0.39 V vs. Li.

Lithium metal is known to suffer from poor coulombic efficiency and severe dendrite growth in conventional electrolytes (30), but because it has the highest gravimetric capacity of all possible anodes (3863 mAh·g⁻¹) there are still numerous efforts to try to enable this anode in a rechargeable battery. Using solvents of low viscosity (31), increased pressure on the electrode (32) and a surface coverage of LiF (33) are all promising methods to improve the lithium metal

anode cyclability and lower the severity of dendrite formation. The exceptionally low viscosity, high vapor pressure and LiF chemical reduction products are all properties inherent to the fluoromethane liquefied gas solvent. To explore the effectiveness of the proposed electrolyte system in enabling the lithium metal anode, the coulombic efficiency of lithium plating and stripping was measured on polished stainless steel electrodes. As shown in Fig. 4B, the fluoromethane based electrolyte shows a stable and high coulombic efficiency of *ca.* 97% over 400 cycles at an aggressive 1 mA·cm⁻² plating and stripping rate with 1 coul·cm⁻² of lithium being passed each cycle. For comparison, a conventional liquid electrolyte system (1 M LiPF₆ in EC:DEC 1:1) is shown to have a poor and unstable coulombic efficiency under identical cell conditions. The comparative fluoromethane and liquid electrolyte lithium plating and stripping cells were stopped at 400 cycles to examine the stainless steel substrates with scanning electron microscopy. The surface morphology of the deposited lithium layer from the fluoromethane based electrolyte is found to be highly uniform with micron sized grain-like features and no evidence of dendrite growth (Fig. 4C). This is in contrast to the highly polymeric and dendritic like surface observed from cycling in the liquid electrolyte (Figure S9). Further, the thickness of the deposited lithium layer in the fluoromethane and comparative liquid electrolyte is found to be *ca.* 60 and 460 μm thick, respectively, reflecting the far superior coulombic efficiency of the novel electrolyte system. The coulombic efficiency for lithium plating and stripping compares with reported values for diethyl ether: tetrahydrofuran 95:5 (98%) (34), 2-methylfuran (97%) (35), and 1,2-dioxolane (98%) (36). The high efficiencies in these systems are only seen with the use of the toxic lithium hexafluoroarsenate (LiAsF₆) salt which is reduced at the lithium metal surface to form a LiF passivation layer. In the fluoromethane system, the solvent itself forms a LiF layer when reduced, which removes the need for LiAsF₆ salt. In addition, the reduction of carbon dioxide to form lithium carbonate has been shown to improve the impedance and cyclability of the lithium metal anode (37), which is used to stabilize the electrode in the present study. More recently, other electrolyte systems have been shown to have high lithium plating and stripping efficiencies without the use of LiAsF₆, but none have demonstrated suitable oxidation stability for use with conventional 4 V cathode systems due to the poor stability at increased potentials of these ether based electrolyte (38). These electrolytes are mostly limited to cathode chemistries which have a low potential and limit the oxidation of these solvents, however, the ability to use a lithium metal anode with a high voltage intercalation cathode would offer a significant increase in energy density as well.

A lithium cobalt oxide (LiCoO₂) cathode was used to

demonstrate the high oxidation stability and compatibility of the fluoromethane based liquefied gas electrolyte with traditional cathode materials. Fluoromethane and conventional liquid based electrolyte systems were used for comparison to test this cathode under identical cell conditions. All charging and discharging of cells was done at a fixed temperature, rather than charging at a higher temperature followed by discharge at a lower temperature. The electrode performance in both electrolyte systems is shown over a number of cycles at various temperatures and C-rates (Fig. 4D) with corresponding voltage vs. discharge capacity curves (Fig. 4E). At +25°C, the discharge capacity at the C/10 rate is very similar, showing *ca.* 133 mAh·g⁻¹ using both electrolytes. At higher rates, the performance of the liquid electrolyte system is marginally higher than the fluoromethane based electrolyte, showing a capacity retention of 87.2% and 81.2% at the 1C rate, respectively. However, at lower temperatures the high rate performance of the fluoromethane based electrolyte is far superior. At -10°C and at the C/10 rate, the fluoromethane and liquid based electrolytes show a 98.3% and 86.2% discharge capacity retention relative to +25°C, respectively. At higher rates or lower temperatures, the liquid based electrolyte fails to cycle properly due to a high cell impedance. In contrast, the cell utilizing the fluoromethane based electrolyte cycles fairly well at higher rates at various temperatures, most notably showing an excellent capacity retention of 60.6% at the C/10 rate at -60°C where traditional liquid electrolytes would generally freeze. This compares favorably with a specially developed low-temperature liquid based electrolyte that shows a discharge capacity retention of 43.5% at the C/10 rate at -60°C using a significantly larger capacity full cell (39). Impedance spectra for cells at each temperature are shown in Figure S10 and fitted parameters given in Table S3. Stability of the fluoromethane based electrolyte system is compared to the liquid electrolyte in Fig. 4F at +25°C and at a C/2 rate. Both electrolytes show very similar stability, with the fluoromethane based electrolyte showing a 96.7% capacity retention after 100 cycles, which demonstrates the high compatibility of this electrolyte system with conventional 4 V cathodes.

The low conductivity of traditional liquid electrolytes is not a primary source of the limited low-temperature performance of Li-ion cells (40). The true origin of these limitations is likely due to charge transfer or solid electrolyte interphase impedance and is sensitive to the type of electrodes and electrolyte used (41, 42). Because identical anodes and cathodes were used in these studies, it is thought the high performance of the fluoromethane based electrolyte at such low temperatures is due to the significantly improved SEI layer on the electrodes. To further explore the electrode-electrolyte interphases seen in the fluoromethane based electrolyte, x-ray photoelectron spectroscopy (XPS)

analysis was conducted on both the lithium metal anode and LiCoO₂ cathodes. As seen in Fig. 5, the surface of lithium metal submerged in fluoromethane is significantly composed of LiF and CH₃Li with a minor Li₂CO₃ signal originating from impurities within the lithium metal. The addition of carbon dioxide to stabilize the surface further adds a significant Li₂CO₃ component to the SEI and lowering of the CH₃Li component, results which agree with the XRD and FTIR analyses. After cycling, the surface components show little chemical change and retain a highly ceramic-like SEI composed primarily of LiF and Li₂CO₃, in contrast to the highly polymer-like SEI formed on the surface on lithium metal submerged in conventional carbonate based electrolytes. The formation of a thin Li₂CO₃ layer via carbon dioxide reduction and the high mobility of lithium ions through the grain boundaries of the highly ceramic surface are thought to both contribute to a substantially decreased impedance through the anode SEI layer. Further, the highly chemically uniform interface as seen in the fluoromethane based electrolyte is thought to contribute to a more uniform current distribution which prevents dendrite formation (43).

While the improvement on the anode is expected to improve cell performance, previous studies have shown that a significantly higher impedance occurs on the cathode, rather than on the anode, at low temperatures (44). The chemistry of the cathode-electrolyte interphase was examined via XPS, shown in Fig. 6. Comparing the XPS spectra of LiCoO₂ electrodes before cycling and after cycling, there are surprising differences. Other than evidence of a small amount of residual LiTFSI salt, there is no change in the Li 1s, C 1s, F 1s and Co 2p spectra for the electrode cycled in the fluoromethane based electrolyte. In contrast, the electrode cycled in the conventional liquid electrolyte shows a significant increase of LiF on the surface of the electrode from decomposition of the PF₆⁻ anion. While the O 1s shows the typical increase in polymeric-type species in agreement with other work (45), the change occurring in the O 1s spectra of the electrode cycled in the fluoromethane based electrolyte is not as clear. Since carbon dioxide is expected to be stable at the potentials seen at this electrode surface and there is no other source of oxygen, the increased peak seen in the O 1s spectra is thought to be due to a change of the surface oxygen of the LiCoO₂ electrode (46) and not related to the formation of an additional surface layer on the electrode. It is concluded that the improved SEI on lithium metal and a cathode with little or no SEI both contribute to the exceptionally high performance at low temperatures of lithium batteries using these liquefied gas electrolytes.

Conclusion

Through a combination of superior physical and chemical properties, hydrofluorocarbon based liquefied gas elec-

trolites are shown to be compatible for energy storage devices. The low melting points and high dielectric-fluidity factors of these liquefied gas solvents allows for exceptionally high electrolytic conductivities over a range of temperatures. High performance in electrochemical capacitors and lithium batteries at temperatures as low as -78°C and -60°C , respectively, has been demonstrated for potential use in aerospace and high-atmosphere applications. Comparable conductivities and performance to conventional electrolytes at moderate temperatures has also been shown, which may be applicable to more mainstream applications such as hybrid and electric vehicles. With the use of difluoromethane as an electrolyte solvent, electrochemical capacitor operation at an increased voltage under accelerated life conditions has been demonstrated, equating to a 23% increase in energy density. With the use of fluoromethane as an electrolyte solvent, a high coulombic efficiency of *ca.* 97% for lithium metal plating and stripping with no evidence of dendritic growth as well as the compatibility with the traditional 4 V LiCoO_2 cathode offers a promising path toward developing a high energy density rechargeable lithium metal battery.

Materials and methods

Materials

Fluoromethane (99.99%) and difluoromethane (99.99%) were obtained from Matheson Gas, fluoroethane (97%), 1,1-difluoroethane (99%), 1,1,1,2-tetrafluoroethane (99%) and 2-fluoropropane (98%) were obtained from Synquest Labs and carbon dioxide (99.9%) was obtained from Airgas. All gases were stored in high pressure refrigerant recovery tanks after use to minimize their release to atmosphere. The salts tetraethylammonium hexafluorophosphate (99.9%) and lithium bis(trifluoromethane)sulfonimide (99.9%) were purchased from BASF while all other salts (electrochemical grade) and acetonitrile (99.8%, anhydrous) were purchased from Sigma-Aldrich. For comparative studies, a liquid electrolyte composed of 1 M LiPF_6 in EC:DEC 1:1 by wt% was used (LP40, BASF). Dimethyl carbonate ($\geq 99\%$, anhydrous) and Nujol Oil for FTIR measurements was purchased from Sigma-Aldrich. Acetonitrile and dimethyl carbonate were dried over molecular sieves prior to use while all other materials were used as received.

For lithium battery electrodes, lithium cobalt oxide, carbon black, and lithium metal were purchased from Sigma-Aldrich, Timcal, and FMC, respectively. In lithium battery and lithium plating and stripping experiments, electrodes were electrically separated by a single porous 20 μm polypropylene separator (Celgard 2075). Commercial electrochemical capacitor jelly rolls (350 F rated) were donated from Maxwell Technologies which had no prior contact with any electrolyte solution.

Electrolytic conductivity measurements

Electrolytic conductivity measurements were performed as detailed previously (47). Briefly, four electrode electrolytic conductivity measurements were performed with a custom fabricated thin-film platinum sputtered electrode on borosilicate glass. The cell constant was calibrated from 0.1 to 100 $\text{mS}\cdot\text{cm}^{-1}$ with a measurement accuracy of $\pm 6\%$. The thin film electrode ensured there would be no geometric change, and hence cell-constant change, under the increased pressures resulting from the studied electrolytes.

Electrochemical capacitors

For electrochemical capacitor testing, jelly rolls were dried overnight under vacuum at $+180^{\circ}\text{C}$. Custom cells were designed to make a four wire measurements to the jelly roll in order to obtain accurate resistance measurements. All metal contacts were made of aluminum to avoid corrosion issues during cell test. Cell assembly was all done under argon atmosphere.

Resistance (DCR) measurements were calculated from the instantaneous iR drop (captured on a high resolution potentiostat) resulting from a 0.5 Amp discharge current after holding at 3 V for 1 hour. Capacitance was measured as

$$\text{Capacitance} = I \cdot (t_2 - t_1) / (V_2 - V_1)$$

where I , V_2 and V_1 were set at -0.5 Amp, 2.4 and 1.2 V, respectively.

Rechargeable lithium metal battery

For rechargeable lithium metal battery testing, electrode slurries composed of LiCoO_2 : carbon black: PVDF binder at a 8:1:1 ratio by weight were mixed with an appropriate amount of N-Methyl-2-pyrrolidone (NMP) solvent and doctor bladed onto 25 μm thick stainless steel 316L foil. The thickness of the coated active electrode after cold calendaring was *ca.* 40 μm thick. Active mass loading was *ca.* 0.9 $\text{mAh}\cdot\text{cm}^{-2}$ or 6.6 $\text{mg}\cdot\text{cm}^{-2}$ (assuming a theoretical capacity of 137 $\text{mAh}\cdot\text{g}^{-1}$ when cycled between 3.5 and 4.1 V). Electrodes of 0.31 cm^2 were used for cell testing. Lithium metal was purchased from FMC and was scrapped clean with a glass slide and rolled with a polyethylene rod to a mirror finish prior to all experiments. Electrodes were electrically separated by a single porous 20 μm polypropylene separator and placed inside a custom fabricated coin cell constructed of high density polyethylene equipped with stainless steel 316L current collectors for both electrodes. All cell assembly was done under an argon atmosphere.

For lithium plating and stripping coulombic efficiency tests, cells were similarly prepared except the LiCoO_2 electrode was not used and lithium was directly plated to the stainless steel 316L current collectors, used here as working electrodes, which were polished to a mirror finish. In all tests, all wetted metal components were stainless steel 316 to avoid corrosion issues.

Electrolyte addition

To form the liquefied gas electrolyte solution, a weighed amount of salt was first pre-loaded into high pressure stainless steel cells along with the capacitor or battery device and sealed under argon atmosphere. The cells were then cooled to a low temperature (*ca.* -60°C) and a controlled amount of solvent was allowed to evaporate from the source and condense into the cell using a mass flow controller (MKS) through a tube connected to the cell, which was then sealed shut with an attached valve. For comparative studies, conventional liquid electrolytes were added under argon atmosphere prior to cell sealing. Cells for comparative study using liquid electrolytes were otherwise mechanically identical to the liquefied gas electrolyte based cells and electrodes were similarly submerged under electrolyte solution.

Thermal and electrochemical characterization

For thermal testing, cells were allowed to thermally equilibrate inside a temperature chamber (Espec) before beginning test. Dry ice was used to cool the cells for tests conducted at -78°C . Temperature measurements were made from a Type K thermocouple with an uncertainty of $\pm 2^{\circ}\text{C}$ and pressure measurements were recorded from a digital pressure transducer (Omega Engineering) with an uncertainty of $\pm 2\%$ of the measured pressure. Temperature and pressure measurements were recorded with a digital data acquisition system (Agilent).

All electrochemical tests were conducted inside high pressure stainless steel cells equipped with electrical feed-throughs which were electrically connected to test electrodes. Cyclic voltammetry experiments were performed with a sweep rate of $1\text{ mV}\cdot\text{sec}^{-1}$. Non-lithium based electrolytes used sputtered platinum counter and reference electrodes. Lithium based electrolytes used lithium metal counter and reference electrodes. All electrolytes used sputtered platinum working electrodes with an area of 1 mm^2 (exposed area defined by a *ca.* 250 nm thick silicon dioxide passivation layer) on borosilicate glass. Separate platinum working electrodes were used for anodic and cathodic potential regions as well as for each temperature to avoid effects from a previous polarization of the working electrode. Potential windows were calculated at the point where current increased beyond $200\text{ }\mu\text{A}\cdot\text{cm}^{-2}$. Battery electrochemical impedance measurements were conducted with a sinusoidal probe voltage of 5 mV and spectra were fitted with ZView software. All electrochemical capacitor cycling, cyclic voltammetry and impedance measurements were conducted with an SP-200 potentiostat (Bio-Logic).

Lithium battery cell cycling was performed with a battery cycler (Arbin). For LiCoO_2 cell tests, cycling consisted of a 100% depth of discharge from 3.5 to 4.1 V for all measurements. For lithium plating and stripping experiments, a single cycle consisted of plating lithium metal to the pol-

ished stainless steel 316L working electrode at a current density of $1\text{ mA}\cdot\text{cm}^{-2}$ with a total charge transfer of $1\text{ coul}\cdot\text{cm}^{-2}$, followed by lithium stripping at $1\text{ mA}\cdot\text{cm}^{-2}$ till the working electrode potential rose above 1 V vs. Li/Li^+ , at which point the current was immediately reversed and the following cycle commenced. The coulombic efficiency was simply calculated as

$$\text{Efficiency \%} = 100 \cdot (Q_{\text{strip}}) \cdot (Q_{\text{plate}})^{-1}$$

where Q_{strip} is the amount of charge passed during the lithium stripping cycle and Q_{plate} is the amount of charge plated ($1\text{ coul}\cdot\text{cm}^{-2}$) each cycle.

Materials characterization

Powder x-ray diffractions (XRD) of samples were collected on a either a Bruker D8 or Bruker D2 Phaser using $\text{Cu K}\alpha$ radiation. Continuous scanning of a detector covering angles from 10.0° to 80.0° with a scan rate of *ca.* $0.02^{\circ}\text{ s}^{-1}$ and wavelength of $\lambda = 0.154\text{ nm}$. Air sensitive samples were sealed under argon atmosphere in polyethylene heat sealed bags and their backgrounds are included in the XRD background spectra.

Fourier transform infrared (FTIR) measurements were conducted with a liquid nitrogen cooled Nicolet 6700 Analytical MCT FT-IR Spectrometer using an Attenuated Total Reflectance (ATR) accessory (single bounce, Diamond/ ZnSe crystal). For lithium metal measurements, samples were submerged into Nujol Mineral oil under an argon atmosphere. The samples were then transferred in a sealed vial then quickly clamped down with a polyethylene plastic backing onto the ATR crystal. This allowed Nujol oil to spread around the sample, protecting it from the atmosphere. Measurements over several minutes were made to ensure there was no change in FTIR spectra due to atmospheric reaction.

Scanning electron microscopy images were taken on a FEI XL30 SFEQ equipped with Ultra High Resolution (UHR) scanning mode at a beam energy of 5 keV . The lithium metal samples imaged were quickly transferred from a vial sealed under argon atmosphere to the SEM chamber to minimize atmospheric exposure. To measure film thickness, a sharp blade was used to cut down the center of the film and the cross section was viewed under SEM at a 30° angle.

X-ray photoelectron spectroscopy measurements were carried out with a AXIS Supra by Kratos Analytical Inc. using monochromatized $\text{Al K}\alpha$ radiation ($h\nu = 1486.7\text{ eV}$) as X-ray source with a base pressure of 10^{-8} Pa . To avoid moisture or air exposure, the XPS spectrometer was directly connected to argon atmosphere filled glove box in which samples were prepared for analysis. The analyzed area of all XPS spectra was $300 \times 700\text{ }\mu\text{m}^2$. XPS was performed with a pass energy of 15 kV and high resolution scans with a step size of 0.05 eV were collected after a survey scan with a step size of 1.0 eV , for lithium 1s, carbon 1s, oxygen 1s, nitrogen

1s, fluorine 1s, and cobalt 2p regions. All of the obtained XPS spectra were analyzed by CasaXPS software and calibrated with a hydrocarbon C 1s signal at 284.6 eV. Core peaks were performed using nonlinear Shirley-type background. The curves were smoothed by a weighted least-squares algorithm and fitted by line shaped composed of 70% Gaussian and 30% Lorentzian. Lithium metal samples were not washed, but in the case of liquid electrolyte, were allowed to dry to remove the majority of the electrolyte from the surface. Cycled LiCoO₂ electrodes were discharged to 3.5 V vs. Li before XPS analysis and were washed with dimethyl carbonate to remove residual salt. Samples were prepped under argon atmosphere.

Numerical calculations

Ionization potentials and electron affinities of solvents were calculated via *ab initio* molecular orbital theory using Gaussian 09W on an isolated molecule in the gas phase. Solvent structures were first geometrically optimized in the ground state at the B3LYP/6-31+g(d,p) level of theory. The ionization potential and electron affinity were calculated from the difference in the electronic energy between the ground state and radical solvent molecules with identical ground state geometry through a vertical electronic transition (Franck-Condon principle). Electrostatic maps of the solvents were visualized via GaussView.

REFERENCES AND NOTES

- R. Fong, U. Von Sacken, J. R. Dahn, Studies of lithium intercalation into carbons using nonaqueous electrochemical cells. *J. Electrochem. Soc.* **137**, 2009–2013 (1990). doi:10.1149/1.2086855
- D. Linden, B. McDonald, The lithium–sulfur dioxide primary battery—its characteristics, performance and applications. *J. Power Sources* **5**, 35–55 (1980). doi:10.1016/0378-7753(80)80094-2
- W. C. West, A. Shevade, J. Soler, J. Kulleck, M. Smart, B. Ratnakumar, M. Moran, R. Haiges, K. O. Christie, G. S. Prakash, Sulfuryl and thionyl halide-based ultralow temperature primary batteries. *J. Electrochem. Soc.* **157**, A571–A577 (2010). doi:10.1149/1.3353235
- E. Zurek, P. P. Edwards, R. Hoffmann, A molecular perspective on lithium-ammonia solutions. *Angew. Chem. Int. Ed.* **48**, 8198–8232 (2009). doi:10.1002/anie.200900373 Medline
- L. Bernard, A. Demortier, J. Lelieur, G. Lepoutre, F. t'Kint de Roodenbeke, A. Le Mehaute, Applications of metal-ammonia solutions to secondary batteries. *J. Phys. Chem.* **88**, 3833–3837 (1984). doi:10.1021/j150661a029
- F. A. Uribe, K. W. Semkow, A. F. Sammells, Cells containing solvated electron lithium negative electrodes. *J. Electrochem. Soc.* **136**, 3559–3565 (1989). doi:10.1149/1.2096509
- A. P. Abbott, C. A. Eardley, J. C. Harper, E. G. Hope, Electrochemical investigations in liquid and supercritical 1, 1, 1, 2-tetrafluoroethane (HFC 134a) and difluoromethane (HFC 32). *J. Electroanal. Chem.* **457**, 1–4 (1998). doi:10.1016/S0022-0728(98)00337-4
- A. P. Abbott, C. A. Eardley, Conductivity of (C4H9) 4N BF4 in liquid and supercritical hydrofluorocarbons. *J. Phys. Chem. B* **104**, 9351–9355 (2000). doi:10.1021/jp0003353
- A. P. Abbott, C. A. Eardley, Electrochemical reduction of CO₂ in a mixed supercritical fluid. *J. Phys. Chem. B* **104**, 775–779 (2000). doi:10.1021/jp9932867
- S. A. Olsen, D. E. Tallman, Conductivity and voltammetry in liquid and supercritical halogenated solvents. *Anal. Chem.* **68**, 2054–2061 (1996). doi:10.1021/ac9511152 Medline
- S. A. Olsen, D. E. Tallman, Voltammetry of ferrocene in subcritical and supercritical chlorodifluoromethane. *Anal. Chem.* **66**, 503–509 (1994). doi:10.1021/ac00076a014
- D. L. Goldfarb, H. R. Corti, Electrical conductivity of decamethylferrocenium hexafluorophosphate and tetrabutylammonium hexafluorophosphate in supercritical trifluoromethane. *J. Phys. Chem. B* **108**, 3358–3367 (2004). doi:10.1021/jp0345102
- D. L. Goldfarb, H. R. Corti, Electrochemistry in supercritical trifluoromethane. *Electrochem. Commun.* **2**, 663–670 (2000). doi:10.1016/S1388-2481(00)00099-0
- M. Ue, K. Ida, S. Mori, Electrochemical Properties of Organic Liquid Electrolytes Based on Quaternary Onium Salts for Electrical Double-Layer Capacitors. *J. Electrochem. Soc.* **141**, 2989–2996 (1994). doi:10.1149/1.2059270
- J. Chmiola, G. Yushin, Y. Gogotsi, C. Portet, P. Simon, P.-L. Taberna, Anomalous increase in carbon capacitance at pore sizes less than 1 nanometer. *Science* **313**, 1760–1763 (2006). doi:10.1126/science.1132195 Medline
- E. Lemmon, M. McLinden, D. Friend, Thermophysical properties of fluid systems. *NIST Chemistry Webbook, NIST Standard Reference Database 69* (National Institute of Standards and Technology, 2005).
- C. A. Kraus, The Electrical Conductivity of Solutions in Methyl Alcohol in the Neighborhood of their Critical Points. II. *Phys. Rev. Ser. I* **18**, 89–103 (1904). doi:10.1103/PhysRevSeriesI.18.89
- M. Barão, N. de Castro, U. Mardolcar, Molecular properties of alternative refrigerants derived from dielectric-constant measurements. *Int. J. Thermophys.* **18**, 419–438 (1997). doi:10.1007/BF02575172
- A. Clifford, T. Clifford, *Fundamentals of supercritical fluids*. (Oxford University Press, 1999).
- A. P. Abbott, C. A. Eardley, R. Tooth, Relative permittivity measurements of 1, 1, 1, 2-tetrafluoroethane (HFC 134a), pentafluoroethane (HFC 125), and difluoromethane (HFC 32). *J. Chem. Eng. Data* **44**, 112–115 (1999). doi:10.1021/je980130b
- E. J. Brandon, W. C. West, M. C. Smart, L. D. Whitcanack, G. A. Plett, Extending the low temperature operational limit of double-layer capacitors. *J. Power Sources* **170**, 225–232 (2007). doi:10.1016/j.jpowsour.2007.04.001
- R. H. Staley, J. Beauchamp, Intrinsic acid-base properties of molecules. Binding energies of lithium (1+) ion to pi- and n-donor bases. *J. Am. Chem. Soc.* **97**, 5920–5921 (1975). doi:10.1021/ja00853a050
- M. Smart, B. Ratnakumar, S. Surampudi, Use of organic esters as cosolvents in electrolytes for lithium-ion batteries with improved low temperature performance. *J. Electrochem. Soc.* **149**, A361–A370 (2002). doi:10.1149/1.1453407
- A. Jänes, E. Lust, Use of organic esters as co-solvents for electrical double layer capacitors with low temperature performance. *J. Electroanal. Chem.* **588**, 285–295 (2006). doi:10.1016/j.jelechem.2006.01.003
- R. Kötz, P. Ruch, D. Cericola, Aging and failure mode of electrochemical double layer capacitors during accelerated constant load tests. *J. Power Sources* **195**, 923–928 (2010). doi:10.1016/j.jpowsour.2009.08.045
- D. Aurbach, Y. Ein-Eli, O. Chusid, Y. Carmeli, M. Babai, H. Yamin, The Correlation Between the Surface Chemistry and the Performance of Li-Carbon Intercalation Anodes for Rechargeable, 'Rocking-Chair' Type Batteries. *J. Electrochem. Soc.* **141**, 603–611 (1994). doi:10.1149/1.2054777
- M. Anouti, Y. R. Dougassa, C. Tessier, L. El Ouatani, J. Jacquemin, Low pressure carbon dioxide solubility in pure electrolyte solvents for lithium-ion batteries as a function of temperature. Measurement and prediction. *J. Chem. Thermodyn.* **50**, 71–79 (2012). doi:10.1016/j.jct.2012.01.027
- G. Di Nicola, F. Polonara, R. Ricci, R. Stryjek, PVTx measurements for the R116+ CO₂ and R41+ CO₂ systems. New isochoric apparatus. *J. Chem. Eng. Data* **50**, 312–318 (2005). doi:10.1021/ja049939g
- J. Desilvestro, S. Pons, The cathodic reduction of carbon dioxide in acetonitrile: An electrochemical and infrared spectroelectrochemical study. *J. Electroanal. Chem. Interfacial Electrochem.* **267**, 207–220 (1989). doi:10.1016/0022-0728(89)80249-9
- D. Aurbach, E. Zinigrad, Y. Cohen, H. Teller, A short review of failure mechanisms of lithium metal and lithiated graphite anodes in liquid electrolyte solutions. *Solid State Ion.* **148**, 405–416 (2002). doi:10.1016/S0167-2738(02)00080-2

31. M. S. Park, S. B. Ma, D. J. Lee, D. Im, S.-G. Doo, O. Yamamoto, A highly reversible lithium metal anode. *Sci. Rep.* **4**, 3815 (2014). [doi:10.1038/srep03815](https://doi.org/10.1038/srep03815) [Medline](#)
32. T. Hirai, I. Yoshimatsu, J. i. Yamaki, Influence of electrolyte on lithium cycling efficiency with pressurized electrode stack. *J. Electrochem. Soc.* **141**, 611–614 (1994). [doi:10.1149/1.2054778](https://doi.org/10.1149/1.2054778)
33. Y. Lu, Z. Tu, L. A. Archer, Stable lithium electrodeposition in liquid and nanoporous solid electrolytes. *Nat. Mater.* **13**, 961–969 (2014). [doi:10.1038/nmat4041](https://doi.org/10.1038/nmat4041) [Medline](#)
34. V. R. Koch, J. L. Goldman, C. J. Mattos, M. Mulvaney, Specular lithium deposits from lithium hexafluoroarsenate/diethyl ether electrolytes. *J. Electrochem. Soc.* **129**, 1–4 (1982). [doi:10.1149/1.2123756](https://doi.org/10.1149/1.2123756)
35. C. Desjardins, T. Cadger, R. Salter, G. Donaldson, E. Casey, Lithium Cycling Performance in Improved Lithium Hexafluoroarsenate/2-Methyl Tetrahydrofuran Electrolytes. *J. Electrochem. Soc.* **132**, 529–533 (1985). [doi:10.1149/1.2113881](https://doi.org/10.1149/1.2113881)
36. Y. Gofer, M. Ben-Zion, D. Aurbach, Solutions of LiAsF₆ in 1, 3-dioxolane for secondary lithium batteries. *J. Power Sources* **39**, 163–178 (1992). [doi:10.1016/0378-7753\(92\)80135-X](https://doi.org/10.1016/0378-7753(92)80135-X)
37. T. Osaka, T. Momma, T. Tajima, Y. Matsumoto, Enhancement of lithium anode cyclability in propylene carbonate electrolyte by CO₂ addition and its protective effect against H₂O impurity. *J. Electrochem. Soc.* **142**, 1057–1060 (1995). [doi:10.1149/1.2044131](https://doi.org/10.1149/1.2044131)
38. J. Qian, B. D. Adams, J. Zheng, W. Xu, W. A. Henderson, J. Wang, M. E. Bowden, S. Xu, J. Hu, J. G. Zhang, Anode-Free Rechargeable Lithium Metal Batteries. *Adv. Funct. Mater.* **26**, 7094–7102 (2016). [doi:10.1002/adfm.201602353](https://doi.org/10.1002/adfm.201602353)
39. M. Smart, B. Ratnakumar, K. Chin, L. Whitcanack, Lithium-ion electrolytes containing ester cosolvents for improved low temperature performance. *J. Electrochem. Soc.* **157**, A1361–A1374 (2010). [doi:10.1149/1.3501236](https://doi.org/10.1149/1.3501236)
40. S. Zhang, K. Xu, T. Jow, Low-temperature performance of Li-ion cells with a LiBF₄-based electrolyte. *J. Solid State Electrochem.* **7**, 147–151 (2003). [doi:10.1007/s10008-002-0300-9](https://doi.org/10.1007/s10008-002-0300-9)
41. B. Ratnakumar, M. Smart, S. Surampudi, Effects of SEI on the kinetics of lithium intercalation. *J. Power Sources* **97-98**, 137–139 (2001). [doi:10.1016/S0378-7753\(01\)00682-6](https://doi.org/10.1016/S0378-7753(01)00682-6)
42. S. Zhang, K. Xu, T. Jow, Electrochemical impedance study on the low temperature of Li-ion batteries. *Electrochim. Acta* **49**, 1057–1061 (2004). [doi:10.1016/j.electacta.2003.10.016](https://doi.org/10.1016/j.electacta.2003.10.016)
43. K. Kanamura, S. Shiraishi, Z. i. Takehara, Electrochemical deposition of very smooth lithium using nonaqueous electrolytes containing HF. *J. Electrochem. Soc.* **143**, 2187–2197 (1996). [doi:10.1149/1.1836979](https://doi.org/10.1149/1.1836979)
44. M. C. Smart, C. Hwang, F. C. Krause, J. Soler, W. C. West, B. V. Ratnakumar, K. Amine, Wide Operating Temperature Range Electrolytes for High Voltage and High Specific Energy Li-Ion Cells. *ECS Trans.* **50**, 355–364 (2013). [doi:10.1149/05026.0355ecst](https://doi.org/10.1149/05026.0355ecst)
45. K. Edström, T. Gustafsson, J. O. Thomas, The cathode–electrolyte interface in the Li-ion battery. *Electrochim. Acta* **50**, 397–403 (2004). [doi:10.1016/j.electacta.2004.03.049](https://doi.org/10.1016/j.electacta.2004.03.049)
46. L. Dahéron, R. Dedryvere, H. Martinez, M. Ménétrier, C. Denage, C. Delmas, D. Gonbeau, Electron transfer mechanisms upon lithium deintercalation from LiCoO₂ to CoO₂ investigated by XPS. *Chem. Mater.* **20**, 583–590 (2007). [doi:10.1021/cm702546s](https://doi.org/10.1021/cm702546s)
47. C. S. Rustomji, J. Mac, C. Choi, T. K. Kim, D. Choi, Y. S. Meng, S. Jin, Thin-film electrochemical sensor electrode for rapid evaluation of electrolytic conductivity, cyclic voltammetry, and temperature measurements. *J. Appl. Electrochem.* **46**, 59–67 (2016). [doi:10.1007/s10800-015-0859-3](https://doi.org/10.1007/s10800-015-0859-3)
48. C. L. Yaws, *Handbook of Vapor Pressure: Volume 4: Inorganic Compounds and Elements*. (Gulf Professional Publishing, 1995), vol. 4.
49. R. D. Nelson Jr., D. R. Lide Jr., A. A. Maryott, “Selected values of electric dipole moments for molecules in the gas phase,” (DTIC Document, 1967).
50. J. Wu, Y. Zhou, An equation of state for fluoroethane (R161). *Int. J. Thermophys.* **33**, 220–234 (2012). [doi:10.1007/s10765-011-1151-3](https://doi.org/10.1007/s10765-011-1151-3)
51. K. Reuter, S. Rosenzweig, E. Franck, The static dielectric constant of CH₃F and CHF₃ to 468 K and 2000 bar. *Physica A* **156**, 294–302 (1989). [doi:10.1016/0378-4371\(89\)90124-6](https://doi.org/10.1016/0378-4371(89)90124-6)
52. M. T. Barão, U. V. Mardolcar, C. A. Nieto de Castro, Dielectric constant and dipole moments of 1, 1, 1-trifluoro-2, 2-dichloroethane (HCFC 123) and 1, 1-difluoroethane (HFC 152a) in the liquid phase. *Fluid Phase Equilib.* **150-151**, 753–762 (1998). [doi:10.1016/S0378-3812\(98\)00356-2](https://doi.org/10.1016/S0378-3812(98)00356-2)
53. X. Meng, X. Gu, J. Wu, S. Bi, Viscosity Measurements of Ethyl Fluoride (R161) from 243 K to 363 K at Pressures up to 30 MPa. *Int. J. Thermophys.* **36**, 2497–2506 (2015). [doi:10.1007/s10765-013-1546-4](https://doi.org/10.1007/s10765-013-1546-4)
54. X. H. Han, Y. J. Xu, X. W. Min, Z. J. Gao, Q. Wang, G. M. Chen, Density data for the refrigerant ethyl fluoride (HFC-161) over a temperature range from (230 to 344) K. *J. Chem. Eng. Data* **56**, 3038–3042 (2011). [doi:10.1021/jp2000827](https://doi.org/10.1021/jp2000827)
55. A. V. Grosse, R. C. Wackher, C. B. Linn, Physical Properties of the Alkyl Fluorides and a Comparison of the Alkyl Fluorides with the Other Alkyl Halides and with the Alkyls of the Elements of Period II. *J. Phys. Chem.* **44**, 275–296 (1940). [doi:10.1021/ji50399a002](https://doi.org/10.1021/ji50399a002)
56. J. Chastain, R. C. King, J. Moulder, *Handbook of X-ray photoelectron spectroscopy: a reference book of standard spectra for identification and interpretation of XPS data*. (Physical Electronics Eden Prairie, MN, 1995).
57. G. F. Meyers, M. B. Hall, J. W. Chinn Jr., R. J. Lagow, X-ray photoelectron spectra of methyl lithium and dilithiomethane. *J. Am. Chem. Soc.* **107**, 1413–1414 (1985). [doi:10.1021/ja00291a052](https://doi.org/10.1021/ja00291a052)
58. E. Kaufmann, S. Sieber, P. R. Schleyer, Carboxylation of lithium compounds: Ab initio mechanisms. *J. Am. Chem. Soc.* **111**, 4005–4008 (1989). [doi:10.1021/ja00193a037](https://doi.org/10.1021/ja00193a037)
59. R. Dedryvère, S. Leroy, H. Martinez, F. Blanchard, D. Lemordant, D. Gonbeau, XPS valence characterization of lithium salts as a tool to study electrode/electrolyte interfaces of Li-ion batteries. *J. Phys. Chem. B* **110**, 12986–12992 (2006). [doi:10.1021/jp061624f](https://doi.org/10.1021/jp061624f) [Medline](#)
60. R. Sharabi, E. Markevich, V. Borgel, G. Salitra, D. Aurbach, G. Semrau, M. A. Schmidt, In situ FTIR spectroscopy study of Li/LiNi_{0.8}Co_{0.15}Al_{0.05}O₂ cells with ionic liquid-based electrolytes in overcharge condition. *Electrochem. Solid-State Lett.* **13**, A32–A35 (2010). [doi:10.1149/1.3292635](https://doi.org/10.1149/1.3292635)
61. D. Aurbach, A. Zaban, A. Schechter, Y. Ein-Eli, E. Zinigrad, B. Markovsky, The study of electrolyte solutions based on ethylene and diethyl carbonates for rechargeable Li batteries I. Li metal anodes. *J. Electrochem. Soc.* **142**, 2873–2882 (1995). [doi:10.1149/1.2048658](https://doi.org/10.1149/1.2048658)
62. D. Aurbach, I. Weissman, A. Schechter, H. Cohen, X-ray photoelectron spectroscopy studies of lithium surfaces prepared in several important electrolyte solutions. A comparison with previous studies by Fourier transform infrared spectroscopy. *Langmuir* **12**, 3991–4007 (1996). [doi:10.1021/ja9600762](https://doi.org/10.1021/ja9600762)
63. Y.-C. Lu, A. N. Mansour, N. Yabuuchi, Y. Shao-Horn, Probing the origin of enhanced stability of “AlPO₄” nanoparticle coated LiCoO₂ during cycling to high voltages: Combined XRD and XPS studies. *Chem. Mater.* **21**, 4408–4424 (2009). [doi:10.1021/cm900862v](https://doi.org/10.1021/cm900862v)
64. J. C. Dupin, D. Gonbeau, H. Benqlilou-Moudden, P. Vinatier, A. Levasseur, XPS analysis of new lithium cobalt oxide thin-films before and after lithium deintercalation. *Thin Solid Films* **384**, 23–32 (2001). [doi:10.1016/S0040-6090\(00\)01802-2](https://doi.org/10.1016/S0040-6090(00)01802-2)
65. R. Dedryvère, H. Martinez, S. Leroy, D. Lemordant, F. Bonhomme, P. Biensan, D. Gonbeau, Surface film formation on electrodes in a LiCoO₂/graphite cell: A step by step XPS study. *J. Power Sources* **174**, 462–468 (2007). [doi:10.1016/j.jpowsour.2007.06.033](https://doi.org/10.1016/j.jpowsour.2007.06.033)
66. L. Dahéron, H. Martinez, R. Dedryvere, I. Baraille, M. Ménétrier, C. Denage, C. Delmas, D. Gonbeau, Surface properties of LiCoO₂ investigated by XPS analyses and theoretical calculations. *J. Phys. Chem. C* **113**, 5843–5852 (2009). [doi:10.1021/jp803266w](https://doi.org/10.1021/jp803266w)
67. W.-T. Tsai, An overview of environmental hazards and exposure risk of hydrofluorocarbons (HFCs). *Chemosphere* **61**, 1539–1547 (2005). [doi:10.1016/j.chemosphere.2005.03.084](https://doi.org/10.1016/j.chemosphere.2005.03.084) [Medline](#)
68. T. L. Brown, M. T. Rogers, The preparation and properties of crystalline lithium alkyls. *J. Am. Chem. Soc.* **79**, 1859–1861 (1957). [doi:10.1021/ja01565a024](https://doi.org/10.1021/ja01565a024)
69. S. Solomon, *Climate change 2007-the physical science basis: Working group I contribution to the fourth assessment report of the IPCC*. (Cambridge University Press, 2007), vol. 4.

ACKNOWLEDGMENTS

This work was supported by Advanced Research Projects Agency–Energy (ARPA-E) the U.S. Department of Energy under award number DE-AR0000646. The authors gratefully acknowledge Prof. Renkun Chen for use of facilities for much of the scope of this work, Prof. Sungho Jin for the helpful discussions, J.Z. Lee for valuable inputs and manuscript review and the kind donation from Maxwell Technologies of their capacitor materials. For the advanced characterization efforts, Y.Y. H.C. and Y.S.M. acknowledge the partial funding support from the Assistant Secretary for Energy Efficiency and Renewable Energy, Office of Vehicle Technologies of the U.S. Department of Energy under the Battery500 consortium. Y.Y. would like to thank I.C. Tran and T. Salk for their help and thoughtful discussions regarding XPS experiments performed at the UC Irvine Materials Research Institute (IMRI) using instrumentation funded in part by the National Science Foundation Major Research Instrumentation Program (Grant CHE-1338173). The SEM analysis in this work was performed at the San Diego Nanotechnology Infrastructure (SDNI) of UC San Diego, a member of the National Nanotechnology Coordinated Infrastructure, which is supported by the National Science Foundation (Grant ECCS-1542148). C.S.R. would like to especially thank the PowerStor team for their support and thoughtful

discussions on electrochemical capacitor technology. All experimental and computational data described in the paper are presented, curated and archived in Cloud Storage system and CommVault Enterprise Backup service. Raw data and meta data are available upon request. Patent applications relating to this work have been filed to date as follows: US Patent Application 15/036,763, European Application 14861242.7 and Provisional Application 62/342,838.

SUPPLEMENTARY MATERIALS

www.sciencemag.org/cgi/content/full/science.aal4263/DC1

Supplementary Text

Figs. S1 to S10

Tables S1 to S4

References (56–69)

17 November 2016; accepted 30 May 2017

Published online 15 June 2017

10.1126/science.aal4263

Cite as: C. S. Rustomji *et al.*, *Science* 10.1126/science.aal4263 (2017).

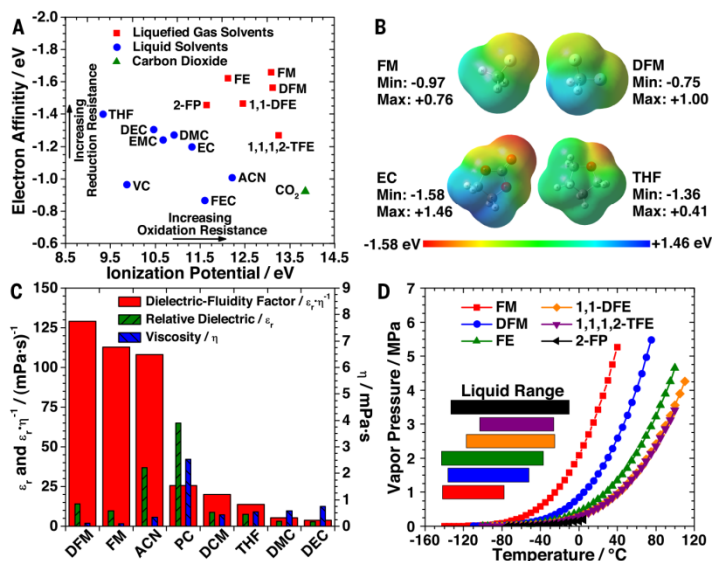


Fig. 1. Physical and chemical properties of liquefied gas solvents. (A) DFT calculated ionization potentials and electron affinities, (B) electrostatic potential maps, (C) relative dielectric, viscosity, dielectric-fluidity values and (D) vapor pressure curves with liquid range of various conventional and liquefied gas solvents. Liquefied gas solvents: fluoromethane (FM), difluoromethane (DFM), fluoroethane (FE), 1,1-difluoroethane (1,1-DFE), 1,1,1,2-tetrafluoroethane (1,1,1,2-TFE), 2-fluoropropane (2-FP). Liquid solvents: acetonitrile (ACN), propylene carbonate (PC), dichloromethane (DCM), tetrahydrofuran (THF), dimethyl carbonate (DMC), diethyl carbonate (DEC), ethyl methyl carbonate (EMC), ethylene carbonate (EC), vinyl carbonate (VC), fluoroethylene carbonate (FEC).

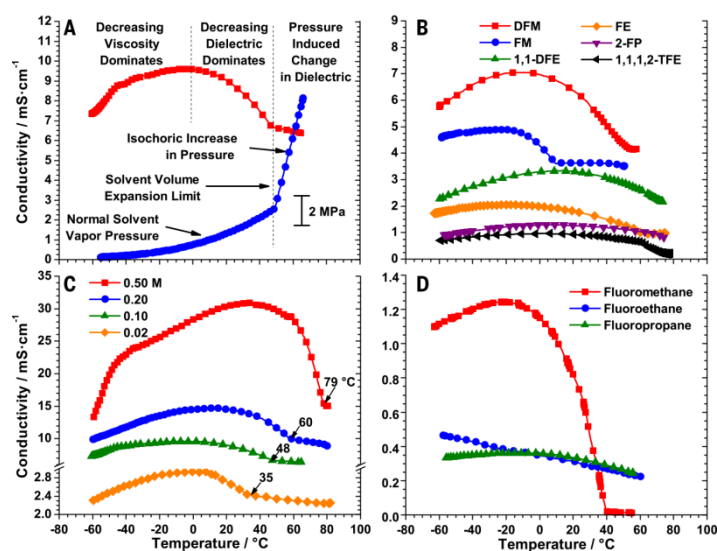


Fig. 2. Electrolytic conductivity over temperature of liquefied gas electrolytes. (A) 0.1 M TBAPF₆ in difluoromethane, (B) 0.1 M EMITFSI in various liquefied gas solvents, (C) TBAPF₆ in difluoromethane at various concentrations and (D) 0.1 M LiTFSI in various monofluorinated liquefied gas solvents.

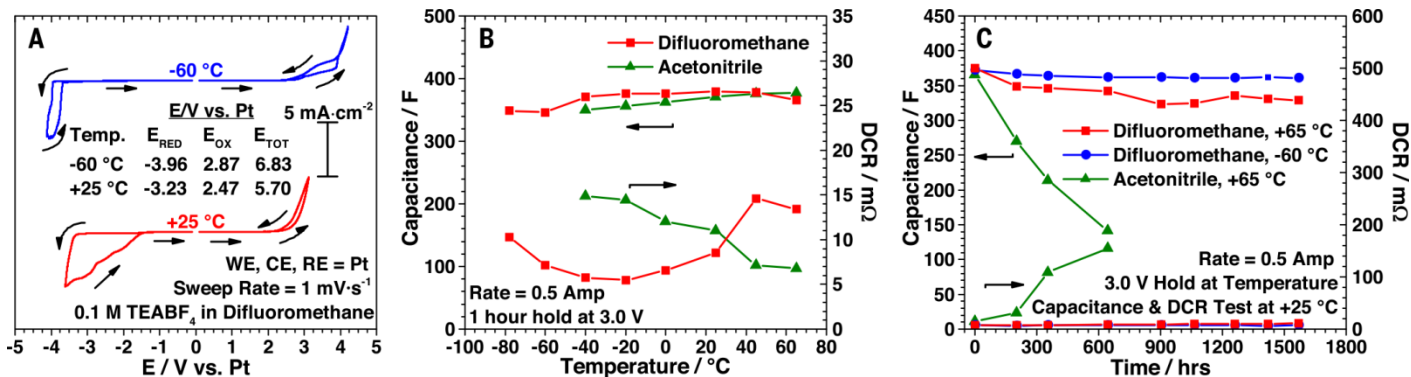


Fig. 3. Electrochemical stability of difluoromethane and its use in electrochemical capacitors. (A) Cyclic voltammograms of 0.1 M TEABF₄ in difluoromethane at +25 and -60°C. Capacitance and resistance measurements of symmetric 350 F electrochemical capacitors using 0.5 M TEABF₄ in difluoromethane and 1 M TEABF₄ in acetonitrile (B) over temperatures from -78 to +65°C and (C) over time with accelerated life testing at 3.0 V at -60 and +65°C. Capacitance was measured from 2.4 to 1.2 V during a constant current discharge. Resistance was measured via the iR drop between voltage hold and constant current discharge steps.

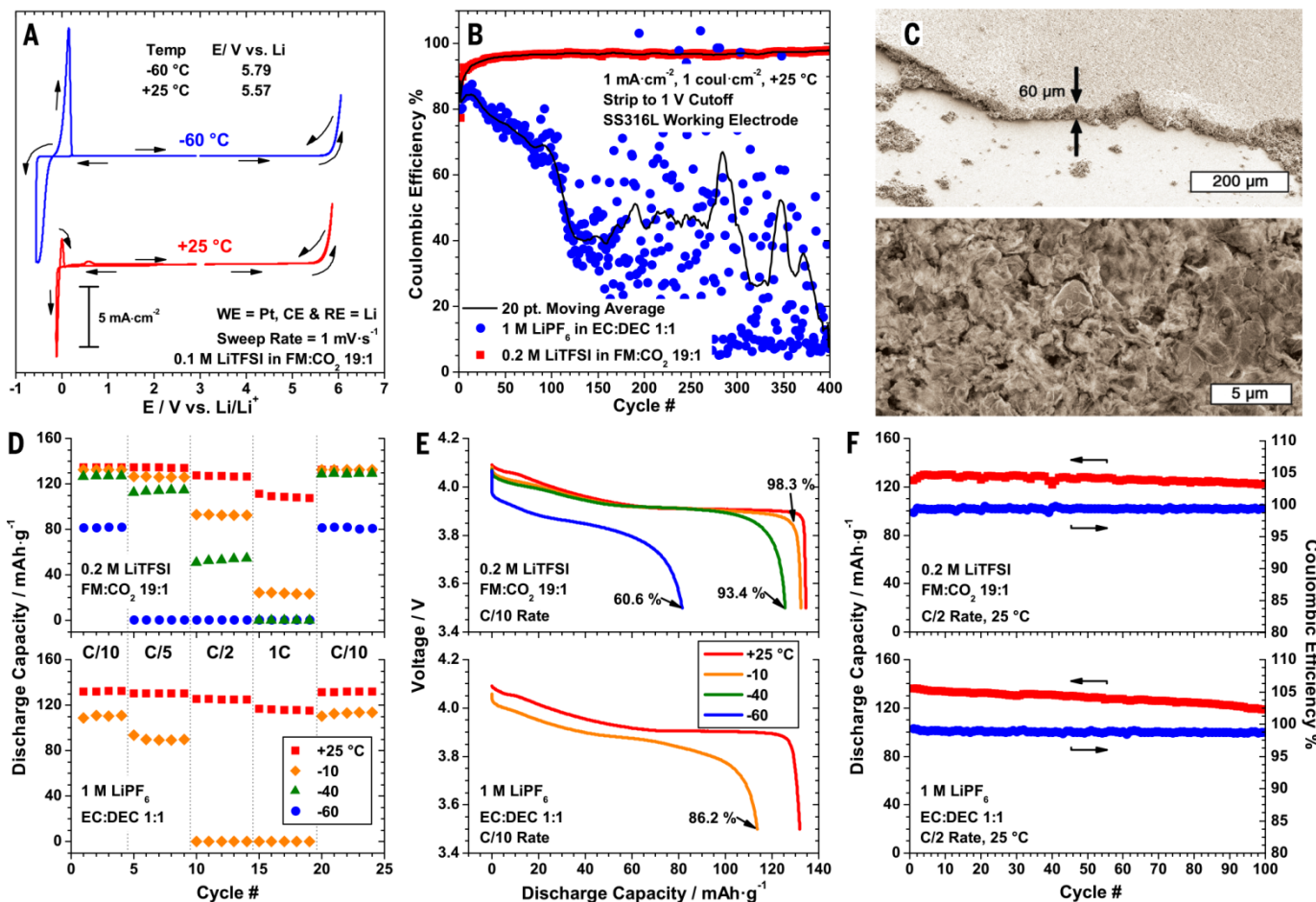


Fig. 4. Electrochemical stability of fluoromethane and its use in lithium batteries. (A) Cyclic voltammograms of 0.1 M LiTFSI in fluoromethane at +25 and -60°C with a voltage sweep rate of 1 mV·sec⁻¹ with oxidation potential limit values taken with a 200 μA·cm⁻² cutoff current. (B) Coulombic efficiency of lithium plating and stripping on a SS316L working electrode over 400 cycles using fluoromethane and conventional liquid based electrolytes at +25°C and (C) SEMs of the fluoromethane SS316L working electrode after the 400 cycles imaged at a 30° tilt in the lithiated state. (D) Discharge capacity over various temperatures and C-rates, (E) voltage vs. discharge capacity over various temperatures at the C/10 rate and (F) discharge capacity and coulombic efficiency with cycling at the C/2 rate of a LiCoO₂ electrode with a lithium metal anode.

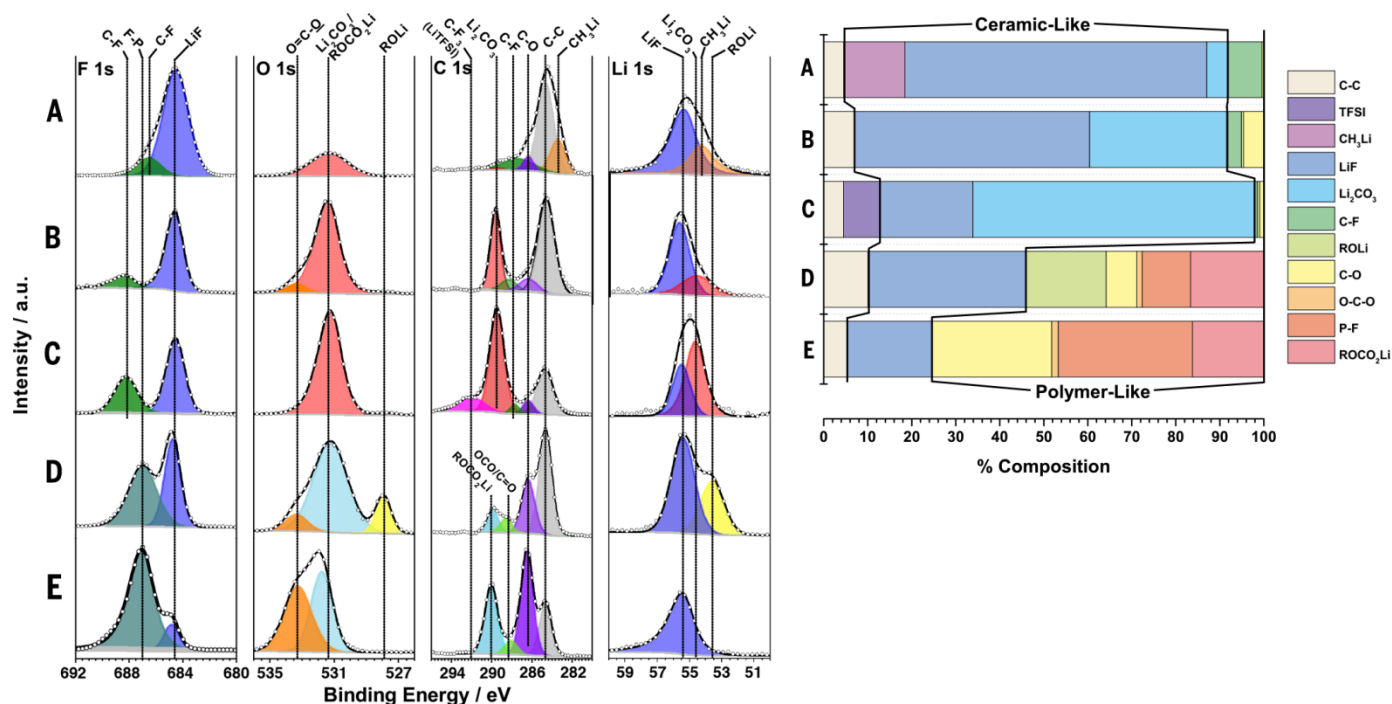


Fig. 5. XPS spectra and calculated percent composition of lithium metal surface products. Lithium metal after being (A) submerged in fluoromethane for three days, (B) submerged in FM:CO₂ 19:1 for three days, (C) cycled 400 times in 0.2 M LiTFSI in FM:CO₂ 19:1, (D) submerged in 1 M LiPF₆ in EC:DEC 1:1 and (E) cycled 400 times in 1 M LiPF₆ in EC:DEC 1:1. No washing of the lithium electrode was done prior to XPS analysis.

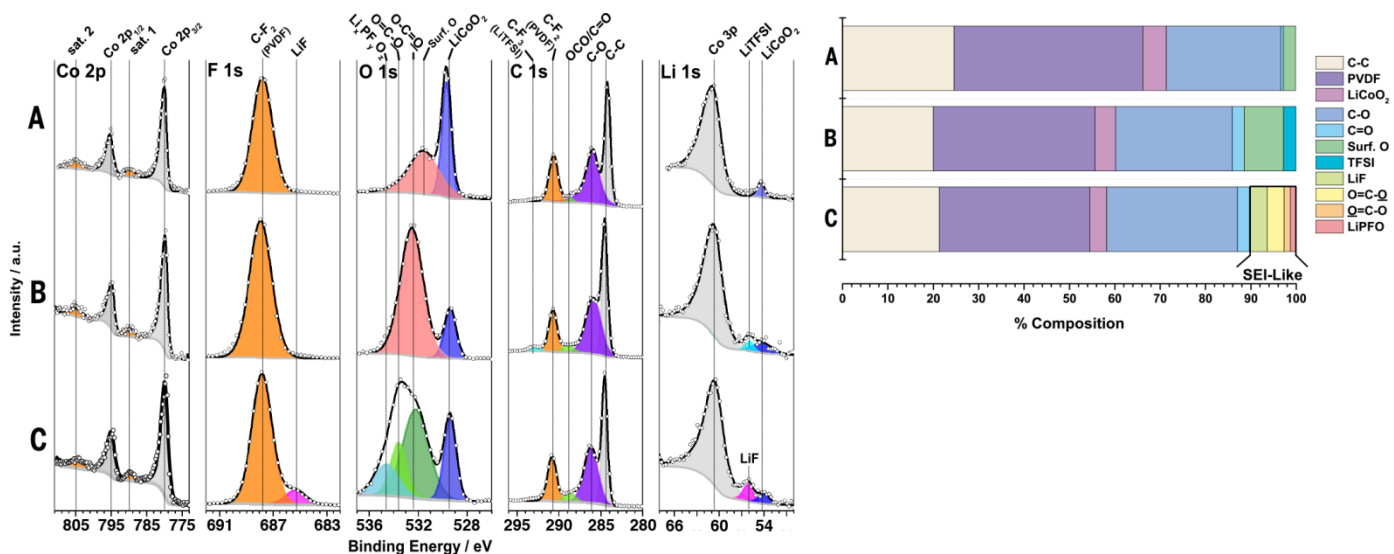
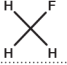


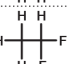
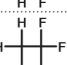
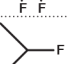


Fig. 6. XPS spectra and calculated percent composition of a LiCoO₂ electrode. Electrodes (A) before cycling and after cycling five times from 3.5 to 4.1 V vs. Li with (B) 0.2 M LiTFSI in FM:CO₂ 19:1 and (C) 1 M LiPF₆ in EC:DEC 1:1. XPS spectra in (B) and (C) were taken in the lithiated state at 3.5 V vs. Li after washing with dimethyl carbonate.

Table 1: Physical properties of the liquefied gas electrolytes studied. Vapor pressure, density, relative dielectric and viscosity values taken as a saturated liquid at +20 °C under saturated vapor pressure, except where noted (8, 16, 18, 48–55).

Solvent	Structure	T_m (°C)	T_b (°C)	T_c (°C)	P_c (MPa)	Vapor Pressure (MPa)	M Wt (g·mol ⁻¹)	Density (g·cc ⁻¹)	Dipole (debye)	Relative dielectric	Viscosity (mPa·s)	$\epsilon_r \cdot \eta^{-1}$ (mPa·s) ⁻¹
Fluoromethane		-142	-78	44	5.90	3.41	34.03	0.599	1.85	9.7	0.085	114
Difluoromethane		-136	-52	78	5.78	1.47	52.02	0.981	1.98	14.2*	0.120	118
Fluoroethane		-143	-38	102	5.01	0.79	48.06	0.707	1.94	—	0.125	—
1,1-Difluoroethane		-117	-24	113	4.52	0.51	66.05	0.912	2.26	12.5†	0.173	72
1,1,1,2-Tetrafluoroethane		-101	-26	101	4.06	0.57	102.03	1.225	2.06	9.7‡	0.207	47
2-Fluoropropane		-133	-9	143	4.20	0.18§	62.09	0.969	—	—	—	—

*20 °C and 2 MPa

†24 °C

‡30 °C

§0 °C

||-9.4 °C

Liquefied gas electrolytes for electrochemical energy storage devices

Cyrus S. Rustomji, Yangyuchen Yang, Tae Kyoung Kim, Jimmy Mac, Young Jin Kim, Elizabeth Caldwell, Hyeseung Chung and Y. Shirley Meng

published online June 15, 2017

ARTICLE TOOLS

<http://science.sciencemag.org/content/early/2017/06/14/science.aal4263>

PERMISSIONS

<http://www.sciencemag.org/help/reprints-and-permissions>

Use of this article is subject to the [Terms of Service](#)

Science (print ISSN 0036-8075; online ISSN 1095-9203) is published by the American Association for the Advancement of Science, 1200 New York Avenue NW, Washington, DC 20005. 2017 © The Authors, some rights reserved; exclusive licensee American Association for the Advancement of Science. No claim to original U.S. Government Works. The title *Science* is a registered trademark of AAAS.